Journal of Inorganic and Organometallic Polymers and Materials (2020) 30:3277–3293
https://doi.org/10.1007/s10904-020-01503-y

Deliberate-Characterization for Ni(II)-Schiff Base Complexes: Promising In-Vitro Anticancer Feature that Matched MOE Docking-Approach

Hana M. Abumelha[1] · Jabir H. Al-Fahemi[2] · Ismail Althagafi[2] · Abrar A. Bayazeed[2] · Zehba A. Al-Ahmed[3] · Abdalla M. Khedr[2,4] · Nashwa El-Metwaly[2,5]

Received: 17 November 2019 / Accepted: 8 March 2020 / Published online: 14 March 2020
© Springer Science+Business Media, LLC, part of Springer Nature 2020

Abstract

A novel series of Ni(II)-Schiff base complexes were synthesized from five hydrazide derivatives. All new synthesizes were fully characterized applying analytical and spectral techniques. 1:1 molar-ratio (M:L) was the main ratio isolated that represented by neutral bi-dentate mode of bonding. Square-planer configuration was the only structural formula proposed for all faintly-colored Ni(II) complexes. Such structural forms were supported by UV–Vis data as well as diamagnetic characteristic. All investigated compounds were configured to reach optimum forms by Gaussian09 program under RTD-B3LYP-FC method. Also, HyperChem (8.1) program was implemented towards Ni(II) complexes to extract QSAR parameters after energy-minimization. Fundamental data were obtained after computational execution, among that which offer a good expectation for Ni(II)-5c, Ni(II)-5d and Ni(II)-5e complexes in aimed application field (therapeutic). MOE-docking approach was considered for all Ni(II) complexes versus 3s7s protein, to signify inhibition-characteristic and rank that. The interaction parameters presented Ni(II)-5c, Ni(II)-5d and Ni(II)-5e complexes, as a best anti-tumor inhibitors, which exactly appeared in laboratory screening.

Keywords Anticancer agent · Ni(ii) complexes · Spectral · MOE docking · Modeling

1 Introduction

Pyridine derivatives have been widely studied for over a century because of their utilization in many branches of chemistry, such as catalysis and therapeutic applications [1]. Many pyridine-containing compounds display fabulous medicinal properties, including hypnotic and sedative [2], HIV antiviral [3], hepatic endoplasmic reticulum calcium uptake regulator [4], α-glucosidase inhibitory, and anticancer activities [5]. Various research studies are continuing to develop and improve specific target-based anticancer drugs in order to reduce drug toxicity, resistance, dosage, and more [6]. Furthermore, benzohydrazide derivatives are considered serious moieties that display great effective inhibitory activity towards several cancer cells [7]. Increasing interest which focused on structural-based therapeutic reagent, designing approach for structure–activity relationships (SAR) was conducted. This will provide excellent rules for the choosing of novel and high active compounds [8], which can be prepared and examined experimentally. Considerable numbers of clinically effective anticancer drugs, are either naturally

Electronic supplementary material The online version of this article (https://doi.org/10.1007/s10904-020-01503-y) contains supplementary material, which is available to authorized users.

✉ Nashwa El-Metwaly
n_elmetwaly00@yahoo.com

[1] Chemistry Department, Faculty of Science, Princess Nourah Bint Abdulrahman University, Riyadh, Saudi Arabia

[2] Department of Chemistry, Faculty of Applied Science, Umm Al-Qura University, Makkah, Saudi Arabia

[3] College of Art and Science, King Khalid University, Dhahran Aljounb, Abha, Saudi Arabia

[4] Chemistry Department, Faculty of Science, Tanta University, Tanta, Egypt

[5] Chemistry Department, Faculty of Science, Mansoura University, Mansoura, Egypt

existing or designed and prepared from other synthetic analogs. Metal complexes display unique characteristics enhancing their active role as promising therapeutic agents, especially as anticancer drugs [9–11]. Great and remarkable characteristics as the ability to produce positively charged ions in aquatic solutions, which may bind with negatively charged biological molecules [12]. The elevated electron affinity of different metal ions can worthy polarize coordinating groups, which droving to propagation of hydrolysis reactions [13]. Recently, significant interest has been oriented to metal-complexes of hydrazides and pyridine based on their biological significant [14]. In recent years, great attention is directed to design and synthesize novel nano-sized metal complexes due to their high potential applicability as anticancer and genotoxic agents [15–17]. In this work we planned to synthesize benzohydrazide derivatives, to be the nucleus for preparing series of their Ni(II) complexes. Descripting molecular and structural formulae of all synthesizes by implementing all available tools was the following step. Theoretical approach was elaborately handled in this study to establish best atomic skeletons or conducts docking simulation. MOE-docking results will be compared deliberately with that resulted from in-vitro screening against breast-cancer cell line, to assess the conformity-extent.

2 Experimental Work

The implemented chemicals and reagents were Merck and PDH from Sigma-Aldrich, also all solvents used were spectroscopic and used as it is without any treatment or purification.

2.1 Synthesis

Synthesis of Ethyl 4-((3-cyano-4,6-dimethylpyridin-2-yl) amino)-benzoate (**3**): To a suspension of 2-chloro-4,6-dimethylnicotinonitrile (**2**) (1.66 g, 0.01 mol) and ethyl *p*-aminobenzoate (1.65 g, 0.01 mol) in ethyl alcohol (30 ml), HCl (1 ml, conc.) was added. The reaction mixture was suffered heating under reflux, for 8 h followed by cooling at 25 °C. The white precipitate formed was filtered off, dried and recrystallized from ethyl alcohol.

White solid, yield 40%, m.p. = 140–141 °C. IR (KBr); 3309 (N–H), 2223 (C≡N), 1712 cm^{-1} (C=O). ^{1}H NMR (DMSO-d_6) (Fig. 1S): 1.31 (t, J = 7.0 Hz, 3H), 2.39 (s, 3H), 2.41 (s, 3H), 4.28 (q, J = 7.0 Hz, 2H), 6.87 (s, 1H, pyridine H-5), 7.74 (d, J = 8.4 Hz, 2H, Ar–H), 7.87 (d, J = 8.4 Hz, 2H, Ar–H), 9.34 ppm (s, 1H, NH). Analysis for $C_{17}H_{17}N_3O_2$; Calcd (Found): C, 69.14 (69.14); H, 5.80 (5.80); N, 14.23 (14.23)%.

Synthesis of 4-((3-Cyano-4,6-dimethylpyridin-2-yl) amino)-benzohydrazide (**4**): To a suspension of ethyl benzoate derivative (**3**) (2.95 g, 0.01 mol) in ethyl alcohol (30 ml), hydrazine hydrate (1 ml, 0.01 mol) was added. The reaction components were heated under reflux for 12 h and then cooled to 25 °C. The precipitate that formed was collected by filtration and then recrystallized from ethyl alcohol.

White crystals, yield 51%, m.p. = 240–242 °C. IR (KBr): 3340, 3287 (NH and NH_2), 2217 (C≡N), 1611 cm^{-1} (C=O). ^{1}H NMR (DMSO-d_6) (Fig. 1S); 2.35 (s, 3H), 2.37 (s, 3H), 4.44 (s, 2H, NH_2), 6.80 (s, 1H, pyridine H-5), 7.65 (d, J = 9.0 Hz, 2H), 7.74 (d, J = 8.0 Hz, 2H), 9.14 (s, 1H, NH), 9.60 ppm (s, 1H, NH). Analysis for $C_{15}H_{15}N_5O$; Calcd. (Found): C, 64.04 (64.15); H, 5.37 (5.34); N, 24.90 (24.96)%.

2.1.1 Synthesis of N′-arylidene-4-((3-cyano-4,6-dimethylpyridin-2-yl)amino)-benzohydrazide 5a–e

A mixture of benzohydrazide derivative (**4**) (0.56 g, 0.002 mol) and 0.002 mol from appropriate para substituted benzaldehyde (namely; benzaldehyde, 4-methylbenzaldehyde, 4-methoxybenzaldehyde, 4-nitro-benzaldehyde and 4-chlorobenzaldehyde) in 20 ml ethyl alcohol, was refluxed for 2 h. The crystalline solid that formed upon cooling was filtered off to afford *N*′-arylidene derivatives (**5a**–**e**).

N′-Benzylidene-4-((3-cyano-4,6-dimethylpyridin-2-yl) amino)-benzohydrazide (**5a**): White solid ($C_{22}H_{19}N_5O$), yield 60%, m.p. = 260–261 °C. IR (KBr); 3412, 3257 (N–H), 2208 (C≡N), 1648 cm^{-1} (C=O).

4-((3-Cyano-4,6-dimethylpyridin-2-yl)amino)-N′-(4-methyl-benzylidene)benzohydrazide (**5b**): White solid ($C_{23}H_{21}N_5O$), yield 56%, m.p. = 270–271 °C. IR (KBr); 3337, 3220 (N–H), 2219 (C≡N), 1640 cm^{-1}(C=O).^{1}H NMR (DMSO-d_6) (Fig. 1S): 2.33 (s, 3H),2.37 (s, 3H), 2.39 (s, 3H), 6.83 (s, 1H, pyridine H-5), 7.26 (d, J = 8.5 Hz, 2H), 7.60 (d, J = 8.0 Hz, 2H), 7.73 (d, J = 8.5 Hz, 2H), 7.85 (d, J = 8.5 Hz, 2H), 8.39 (s, 1H, CH = N), 9.27 (s, 1H, NH), 11.67 ppm (s, 1H, NH).

4-((3-Cyano-4,6-dimethylpyridin-2-yl)amino)- N′-(4-methoxy-benzylidene)benzohydrazide (**5c**): White solid($C_{23}H_{21}N_5O_2$), yield 55%, m.p. > 300 °C.IR (KBr): 3331, 3252 (N–H), 2219 (C≡N), 1638 cm^{-1}(C=O).^{1}H NMR (DMSO-d_6) (Fig. 1S); 2.39 (s, 3H), 2.41 (s, 3H), 3.81 (s, 1H, OCH_3), 6.85 (s, 1H, pyridine H-5), 7.02 (d, J = 8.4 Hz, 2H), 7.67 (d, J = 8.4 Hz, 2H), 7.75 (d, J = 8.4 Hz, 2H), 7.86 (d, J = 8.4 Hz, 2H), 8.39 (s, 1H, CH = N), 9.25 (s, 1H, NH), 11.60 ppm (s, 1H, NH).

4-((3-Cyano-4,6-dimethylpyridin-2-yl)amino)-N′-(4-nitrobenzylidene)-benzohydrazide (**5d**): Yellow solid ($C_{22}H_{18}N_6O_3$), yield 78%, m.p. = 295–298 °C. IR (KBr): 3292, 3206 (N–H), 2228 (C≡N), 1666 cm^{-1}(C=O). ^{1}H NMR (DMSO-d_6) (Fig. 1S); 2.38 (s, 3H), 2.40 (s, 3H), 6.86 (s, 1H, pyridine H-5), 7.75 (d, J = 9.0 Hz, 2H), 7.87 (d, J = 8.0 Hz,

2H), 7.98 (d, J = 8.0 Hz, 2H), 8.29 (d, J = 9.0 Hz, 2H), 8.52 (s, 1H, CH = N), 9.30 (s, 1H, NH), 12.03 ppm (s, 1H, NH).

N′-(4-Chlorobenzylidene)-4-((3-cyano-4,6-dimethylpyridin-2-yl)-amino)benzohydrazide (**5e**): White solid ($C_{22}H_{18}ClN_5O$), yield 71%, m.p. = 269–270 °C. IR (KBr); 3302, 3214 (N–H), 2209 (C≡N), 1660 cm^{-1}(C=O). MS *m/z* (%) (Fig. 2S); 405 (M^+ + 2, 10.26), 404 (M^+ + 1, 43.47), 403 (M^+, 100.00), 251 (16.44), 250 (32.45), 90 (17.43), 77 (10.27).

2.1.2 Synthesis of Ni(II)-Schiff Base Complexes

Ethanolic solution of 2 mmol from each N′-arylidene ligand **5a–e** (0.739, 0.767, 0.799, 0.829 and 0.808 g, sequentially) was added to ethanolic $NiCl_2.6H_2O$ (0.334, 2 mmol) solution. The reaction mixtures were heated under reflux for 2–3 h. 0.5 g of sodium acetate were added to each reaction-mixture to precipitate the aimed Ni(II) complexes. The faint colored complexes (yellow or orange) were isolated by filtration and washed by EtOH and ether, then kept to dray in desiccator under $CaCl_2$. All isolated complexes are stable, non-hygroscopic and have high m.p. (˃ 300 °C).

2.2 CT-DNA Binding Methodology

The binding-grade of Ni(II)-Schiff base complexes toward CT-DNA (calf thymus), was screened by applying spectrophotometric titration technique. Amount of CT-DNA (50 mg) was dissolved in bi-distilled water at pH = 7 by a constant stirring and kept overnight at 4 °C. Mixing of 5.0 mM of tris(hydroxymethyl)-aminomethane with NaCl (50 mM) dissolved in bi-distilled water at pH = 7, yields Tris–HCl buffer. A stock solution of DNA was prepared in Tris–HCl buffer, the absorbance of this solution was measured at 260 and 280 nm, the ratio of A260/A280 recorded at 1.8–1.9 range. That points to pure DNA solution, which free from protein [18]. A concentration of DNA-stock solution (5.25×10^{-4} M), was determined by knowing molar absopititvity-coefficient value ($\varepsilon = 6600\ M^{-1}\ cm^{-1}$) at 260 nm. 2.5×10^{-5} M was the concentration used from each complex, which faced a gradual additive from CT-DNA amount that covering concentration range upon 0.00 to 1.58×10^{-4} mol l^{-1}. The blank solution includes all quantitative additives (buffer and DNA) except the tested compound (complex), which be used as a reference, to cancel the absorption of DNA. Using 1 cm quartz cuvette, the absorption of each concentration was measured over 200–900 nm range at 25 °C versus blank solution cell. The binding constant (K_b) for each tested complex towards DNA, was estimated by the following equation; $[DNA]/(\varepsilon a - \varepsilon f) = [DNA]/(\varepsilon b - \varepsilon f) + 1/K_b\ (\varepsilon a - \varepsilon f)$ [19], through relation between slope/intercept, from the plots of $[DNA]/(\varepsilon a - \varepsilon f)$ vs.[DNA]. Where; the molar concentration of DNA is [DNA], the extinction coefficient observed is εa = Aobs/[compound] at definite [DNA]. Also, εf is the extinction-coefficient for each free Ni(II) complex, εb is the extinction-coefficient of the complex at full-bonding towards DNA.

2.3 Computational Studies

2.3.1 Conformational Strategy

The optimized structural forms for all new compounds were demonstrated over Gaussian 09 program-screen [20] after choosing the appropriate method. According to polarizable model, a default ethanol solvent was used for configuration process upon DFT/B3LYP method. 3-21G was the diffusion function basis set suitable for Schiff base derivatives and their Ni(II) complexes [16, 17]. The yielded files (log and chk) facilitate estimating significant indexes, which lead to broad visualization for their discriminated characteristics. All optimized structures were visualized over Gauss-View program [21], for schematic numbering and other significances. Such significances were obtained based on frontier energy-gaps (ΔE) by utilizing standard equations [22, 23].

2.3.2 Molecular Operating Environmental-Docking (MOE) Approach

MOE docking (vs. 2015) approach is the most recent software concerning with docking simulation technique that aims to evaluate the inhibition extent towards pathogen-proteins. Elected protein was 3s7s, as the PDB file of crystal structure for human placental aromatase complexed to breast cancer drug [24]. This simulation technique was implemented for all new synthesizes starting with the orientation till optimization for tested compound. The pre-optimization configuration was achieved by adding hydrogen atoms, atomic charges and potential energies. In addition to, important parameters were adjusted by MMFF94x force field during energy minimization [16, 17, 24]. The configured compounds were saved as MDB format that know ready for docking process. The orientation of 3s7s protein was the following interest which started by built hydrogen atoms over receptors after removing water molecules. Automatically connecting the receptor types followed by fixing the potential energies, were the second stage. Site-finder was done over line helix of protein amino acids [25]. The dummies were adjusted over alpha-sites in protein and then the docking process can be started. The docking simulation process consumed variable times covering all tested compounds but all processes were the average of 30 poses. Such poses were adjusted by London dG scoring function that improved twice by triangle Matcher methods. The binding rank was discriminated among the tested compounds through scoring energy values. Meanwhile, ligand type, receptors, interaction

type, H-bond length and energy content were the other features recorded for docked complexes. The influential effect of H-bond length (≤ 3.5 Å) was extended to be the most significant judger on the magnitude of interaction validity at all. Moreover, the interaction patterns as well as the surface maps were also extracted to confirm comparative features.

2.4 Anticancer Screening

In National Research Centre of Egypt, this screening was executed at Bioassay-Cell Culture Laboratory. Using 3-(4,5-dimethylthiazol-2-yl)-2,5-diphenyltetrazolium bromide (MTT) assay method, the cytotoxic efficiency of new Ni(II)-Schiff base complexes, were evaluated [26]. From ATCC (American Type Culture Collection, USA) Tissue culture Unite, MCF-7 cell line was purchased. In sterile area of laminar flow-cabinet safety-class (Baker, SG403INT, Sanford, ME, USA), this investigation procedure was done. At 37 °C under 5% CO_2, MCF-7 cell, was suspended in medium of DMEM from 1% mixture of antibiotic–antimycotic (10,000 U ml^{-1} Potassium Penicillin, 10,000 µg ml^{-1} Streptomycin Sulfate and 25 µg ml^{-1} Amphotericin B) and 1% L-glutamine. Using water jacketed carbon dioxide incubator (Sheldon, TC2323, Cornelius, OR, USA)at37 ºC, the cell batch was cultured for 10 days, then seeded by 10×10^3 cells/well in fresh medium for complete growth (96-well microtiter plastic plates) under 5% CO_2. After aspirating media cultivated, fresh medium was added (without serum) and cells were incubated alone (negative control) or by variable concentrations from tested samples (in DMSO) till reaching, 100, 50, 25, 12.5, 6.25, 3.125, 0.78 and 1.56 µg ml^{-1} (final concentrations). Then and after incubation for 48 h the medium was aspirated and 40 µl MTT salt (2.5 µg ml^{-1}) were added. Such addition was carried out on each well which still incubated along further 4 h under 5% CO_2 at 37 °C. 200 µl of 10% Sodium dodecyl sulphate (SDS) prepared in deionized water, were added to each well to stop the reaction and dissolving the crystals formed, then incubated overnight at 37 °C. Cytotoxic natural agent (positive control) composes of 100 µg ml^{-1}, gives 100% lethality under the same conditions [26–28]. The absorbance was measured at 595 nm (reference λ = 620 nm) using microplate multi-well reader (Bio-Rad Laboratories Inc., model 3350, Hercules, California, USA). Implementing independent t-test by SPSS 11 program, the statistics were tested for samples versus negative control (cells with complexes). The viability percentage was calculated using the following relation; (Reading of extract/Reading of negative control) − 1) × 100.

2.5 Analysis Techniques

The analytical techniques implemented in this study to analyze all new synthesizes (ligands and Ni(II) complexes) were schematically depicted (Scheme 1S). Evaluation of nickel and chloride content was carried out by complexometric and gravimetric analysis, respectively using standard procedures [29].

3 Results and Discussion

Analytical results proposed equi-molar ratio, for all Ni(II) complexes except of Ni(II)-5d complex, which has 1:2 ratio (M:L). Analytical and physical characteristic were summarized in Table 1. The molar conductivity values (Λ_m, 10^{-3} M) were measured for four Ni(II) complexes that displayed excellent solubility in solvent (DMSO). The non-conducting feature was efficiently prevailed with all measured complexes except Ni(II)-5e [30]. The conducting appearance of Ni(II)-5e complex was suggested based on Λ_m value (48.93 $\Omega^{-1}cm^2\ mol^{-1}$). This value matches with presence of ionizable chloride ion, which expelled outer coordination sphere after the presence of water molecule. The inductive effect of p-substituents play significant role on coordination behavior which led to different molecular formula (will be discussed in detail later).

3.1 Synthesis mechanism of Schiff bases

This study started by synthesis of 4,6-dimethyl-3-cyano-pyridin-5-one (**1**) from acetylacetone and cyanoacetamide in ethyl alcohol and potassium carbonate [31], (Scheme 1). Heating pyridine compound (**1**) with phosphorus oxychloride, furnished by 2-chloro-4,6-dimethylnicotinonitrile (**2**) [31].

The chlorine atom of 2-chloronicotinonitrile derivative **2** proved to be reactive towards nucleophilic-substitution by nitrogen-nucleophile such as; ethyl 4-aminobenzoate to afford ethyl 4-(3-cyano-pyridin-2-ylamino)benzoate scaffold (**3**) (Scheme 2). The compatible elemental and spectral analysis supported the proposed structure of benzoate compound (**3**). Its IR spectrum displayed absorptions at 3309, 2223 and 1712 cm^{-1} to indicate the presence of N–H, nitrile (C≡N) and carbonyl of ester (COOEt) groups. The ^1H NMR signals were identified as triplet at 1.31 ppm and quartet at 4.28 ppm for the protons of ethoxy group (–O–CH_2–CH_3). The singlet-signals at 2.39 and 2.41 ppm assign for methyl groups-protons. The proton of pyridine C-5 resonated as singlet at 6.87 ppm, while the aromatic protons appeared as two doublet signals at 6.74 and 7.87 ppm. The proton of N–H function resonated as singlet at 9.34 ppm. The hydrazide derivative (**4**) was achieved by refluxing ethyl 4-(3-cyano-pyridin-2-ylamino) benzoate compound (**3**) with hydrazine hydrate in EtOH for 2 h. The structure of compound (**4**) was confirmed by spectroscopic techniques including IR and mass spectral analysis. Its IR spectrum

Table 1 Analytical and physical characteristics of Schiff bases (**5a–e**) and their Ni(II) complexes

Compounds (empirical formula/ found)	Λ_m (Ohm^{-1} cm^2 mol^{-1})	Color	Elemental analysis (%) calcd. (found)				
			C	H	N	Ni	Cl
(1) HL(BDAB, **5a**) ($C_{22}H_{19}N_5O$) (369.42/369.04)	–	Creamy-white	71.53 (71.55)	5.18 (5.16)	18.96 (18.96)	–	–
(2) $[NiCl_2(HL)]\cdot 2H_2O$ (535.05)	6.13	Yellow	49.39 (49.39)	4.33 (4.24)	13.09 (13.04)	10.97 (10.98)	13.25 (13.25)
(3) HL(CDAB, **5b**) ($C_{23}H_{21}N_5O$) (383.45)	–	Creamy-white	72.04 (72.03)	5.52 (5.50)	18.26 (18.26)	–	–
(4) $[NiCl_2(HL)]\cdot 2H_2O$(549.08)	7.29	Yellow	50.31 (50.31)	4.59 (4.55)	12.75 (12.70)	10.69 (10.69)	12.91 (12.92)
(5) HL (CDMB, **5c**) ($C_{23}H_{21}N_5O_2$) (399.45)	–	Creamy-white	69.16 (69.20)	5.30 (5.32)	17.53 (17.55)	–	–
(6) $[NiCl_2(HL)]\cdot H_2O$(547.06)	7.77	Yellow	50.50 (50.48)	4.24 (4.23)	12.80 (12.83)	10.73 (10.73)	12.96 (12.95)
(7) HL(CDNB, **5d**) ($C_{22}H_{18}N_6O_3$) (414.42)	–	Yellow	63.76 (63.77)	4.38 (4.37)	20.28 (20.30)	–	–
(8) $[NiCl_2(HL)_2]$ (958.43/958.94)	–	Orange	55.14 (55.17)	3.79 (3.81)	17.54 (17.57)	6.12 (6.11)	7.40 (7.41)
(9) HL(CCDB, **5e**) ($C_{22}H_{18}ClN_5O$) (403.86)	–	Creamy-white	65.43 (65.40)	4.49 (4.52)	17.34 (17.34)	–	8.78 (8.77)
(10) $[NiCl(HL)(H_2O)]Cl$ (551.48/534.34)	48.93	Orange	47.91 (48.05)	3.66 (3.49)	12.70 (12.72)	10.64 (10.67)	19.29 (19.32)

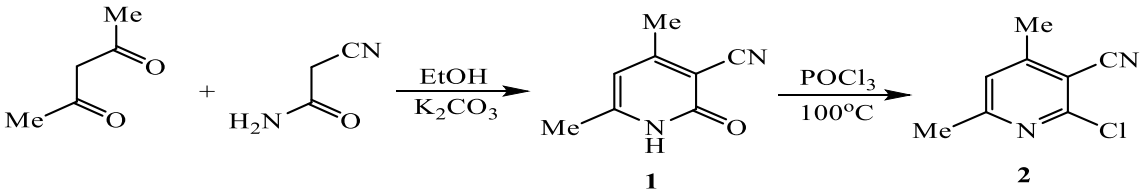

Scheme 1 Mechanism of Schiff bases synthesis

Scheme 2 Synthesis of N′-arylidene-4-((3-cyano-4,6-dimethylpyridine-2-yl) amino)-benzohydrazide Schiff bases **(5a–e)**

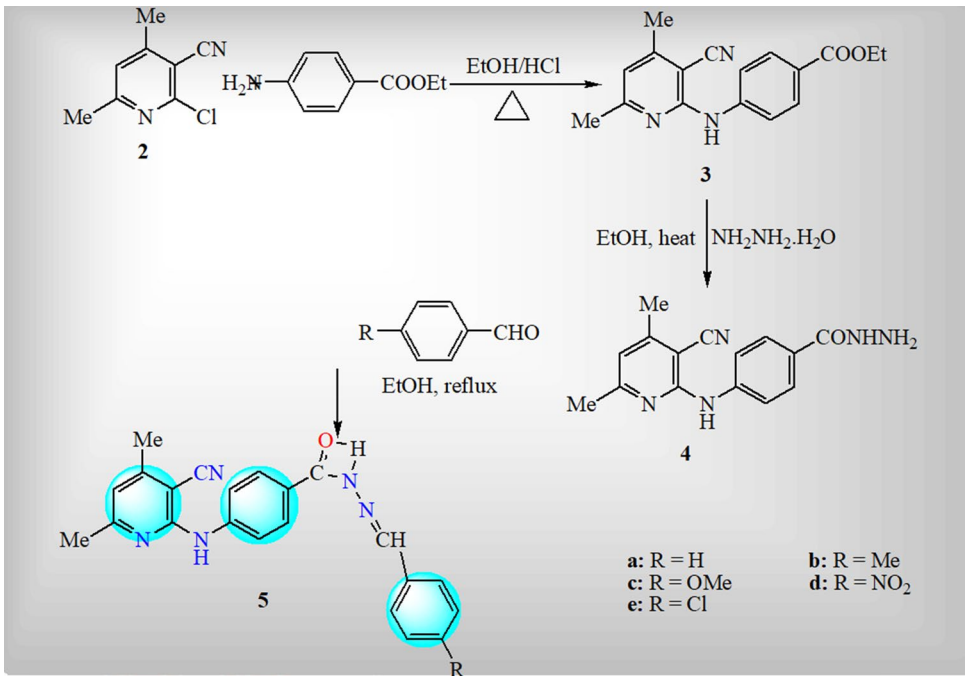

exhibited absorption bands at 3340 and 3287 cm^{-1} for N–H stretching of NH and NH_2 groups. The absorptions at 2217 and 1611 $cm^{-1}$are referring to nitrile (C≡N) and carbonyl (N–C=O) groups, respectively. ^{1}H NMR spectrum indicated the absence of any signal related to ethoxy group and displayed singlet signals of hydrazide moiety ($CONHNH_2$) at 4.44 ppm (NH_2) and 9.14 ppm (NH). Condensation of hydrazide (**4**) with different aromatic benzaldehydes (benzaldehyde, 4-methylbenzal-dehyde, 4-methoxybenzaldehyde, 4-nitrobenzaldehyde and 4-chlorobenzaldehyde) proceeded by boiling in EtOH to afford Schiff's bases (**5**). The structure of **5** was confirmed because of their spectral data and satisfactory elemental analysis. Their IR spectra showed absorption band at wave number ranged from 1638 to 1666 cm^{-1}corresponding to carbonyl group. The proton of azomethine group (N–N = CH–) resonated as singlet signal in ^{1}H NMR spectra in the range of 8.39–8.52 ppm.

3.2 Comparative Vibrational Study

The synthesized Schiff base ligands appeared favorable for neutral bi-dentate binding-mode in most Ni(II) complexes. This appearance was supported by the state of functional-group bands (Table 2), which attributing to, υ(NH), υ(C=O), υ(C=N)pr, υ(C=N^{21}–N) and υ(CN) [32]. More or less unshifted vibrational-bands that assign for nitrile and pyridine (C=N) groups, asserts on their ruling-out from coordination (Fig. 3S). Mostly, lower shifted appearance for υ(C=O) and υ(C=N^{21}) was recorded, except with Ni(II)-5d spectrum that favor the excluding of N^{21} from contribution. Neutral monodentate mode of bonding was proposed for (**5d**)derivative, which sounds preferable in presence of highly inductive p-substituted group (NO_2). Such group caused electron deficient suffered by close functional-groups especially that contributing in resonance. The exclusion of C=N^{21} group, was expected and supported by un-changeable band at 1604 cm^{-1}[33]. Ni(II)-5d complex was appeared by unique molar-ratio (1 M:2L) although high steric hindrance, which was not obstacle for this ratio. This proposal was confirmed firstly by analytical data (elemental and mass spectrum) and asserted by IR spectrum, which exhibited the bands by noticeable raise in intensity. The high covalent feature of conjugated anion (chloride) devotes the covalent attachment of the two atoms in all complexes, except for Ni(II)-5e. This is due to the competition of chloride atom with one water molecule that always overcome and contributing. This feature was supported electrically, through the conductivity measurements for 10^{-3} M, which displayed value agrees with conducting feature for mono-anion. Water molecules were proposed attached physically or chemically with coordination sphere, through the appearance of new bands assign for $\delta_r(H_2O)$and $\delta_w(H_2O)$ [34]. Such was supported by TGA analysis, which will be discussed later. υ(Ni–N) and υ(Ni–O) vibrational-bands were recorded at lower wavenumber region, to confirm new bond types between ligand and nickel atom [35].

3.3 UV–Vis Spectral-Data

Electronic spectral analysis as well as magnetic moment measurement (Table 3) were considered the most significant to recognize and discriminate structural formulae of transition metal complexes. This study was achieved in DMSO solvent over broad UV–Vis spectral-range (200–1200 nm), which covering allowed and forbidden transitions [36]. The diamagnetic feature ($\mu_{eff} = 0$) of all investigated complexes beside their faint colors (yellow or orange), likely emphasizes square-planer configuration. Electronic transition spectra of all Ni(II)-Schiff base complexes (Fig. 4S), exhibited bands according to intra-ligand, charge transfer and ligand field transitions. The $\pi \rightarrow \pi^*$ and $n \rightarrow \pi^*$were the intra-ligand transitions, which appeared at 33,259, – 30,303 and 31,250–26,315 cm^{-1} ranges, respectively [37]. While, the bands appeared

Table 2 Functional IR-bands (cm^{-1}) of Schiff bases (**5a–e**) and their Ni(II) complexes

Compounds	$\nu_{(OH)}$	$\delta_{(NH)s}$	$\nu_{(C=O)}$	$\nu_{(C=N)s}$	$\nu_{(CN)}$	$\delta_{(OH)}$	δ_r and δ_w (H_2O)	ν_{M-O}	ν_{M-N}
(1) HL(BDAB, **5a**)	–	3412, 3257	1648	1611, 1562	2208	–	–	–	–
(2) $[NiCl_2(HL)]\cdot 2H_2O$	B. c. at 3415	1612	1544, 1565	2211	1364	850, 687	590	467	
(3) HL(CDAB, **5b**)	–	3337, 3220	1640	1610, 1534	2219	–	–	–	–
(4) $[Ni\ Cl_2(HL)]\cdot 2H_2O$	B. c. at 3406	1613	1585, 1563	2213	1361	808, 701	588	484	
(5) HL(CDMB, **5c**)	–	3331, 3252	1638	1610, 1532	2219	–	–	–	–
(6) $[Ni\ Cl_2(HL)]\cdot H_2O$	B. c. at 3363	1612	1591, 1564	2210	1306	824, 699	585	502	
(7) HL(CDNB, **5d**)	–	3292, 3206	1666	1604, 1561	2228	–	–	–	–
(8) $[NiCl_2(HL)_2]$	–	3289, 3207	1666	1605, 1561	2231	–	–	606	–
(9) HL(CCDB, **5e**)	–	3302, 3214	1660	1609, 1538	2209	–	–	–	–
(10) $[NiCl(HL)(H_2O)]Cl$	3414	3338, 3215	1613	1586, 1563	2213	1363	819, 699	587	485

B. c. broad centered

Table 3 Electronic transition bands (cm^{-1}) of Ni(II)-Schiff base complexes

Complexes	Dq (Δ/10)	d–d transition bands	Charge transfer bands and intra-ligand transitions	Proposed geometry
(1) [Ni Cl_2(HL)]·$2H_2O$	1989.5	19,895	33,333; 25,000; 23,809	Square-planer
(2) [Ni Cl_2(HL)] ·$2H_2O$	2000.0	20,000; 12,500; 11,000	30,303; 26,315; 25,000	Square-planer
(3) [Ni Cl_2(HL)] ·H_2O	1960.7	19,607; 16,380	32,310; 28,571; 25,000	Square-planer
(4) [$NiCl_2(HL)_2$]	1923.0	19,230; 15,385	33,300; 31,250; 23,256	Square-planer
(5) [NiCl(HL)(H_2O)]Cl	1923.3	19,233; 16,129	33,259; 29,850; 24,814	Square-planer

at 25,000–23,256 cm^{-1} range, signify Ni–O and Ni–N charge transfer [38]. Regarding ligand-field transitions of d^8-systems in square-planer configuration, which represented d_z^2 as a ground orbital, were clearly remarked and assigned. Bands recorded at 19,230–20,000 and 12,500–16,380 cm^{-1} ranges are assigning to $^1A_1g \rightarrow {}^1A_2g$ and $^1A_1g \rightarrow {}^1B_1g$ transitions, respectively in square-planer geometry (Fig. 1). While, the band recorded at 11,000 cm^{-1} in Ni(II)-5b complex-spectrum, refers to spin-forbidden transition [39].

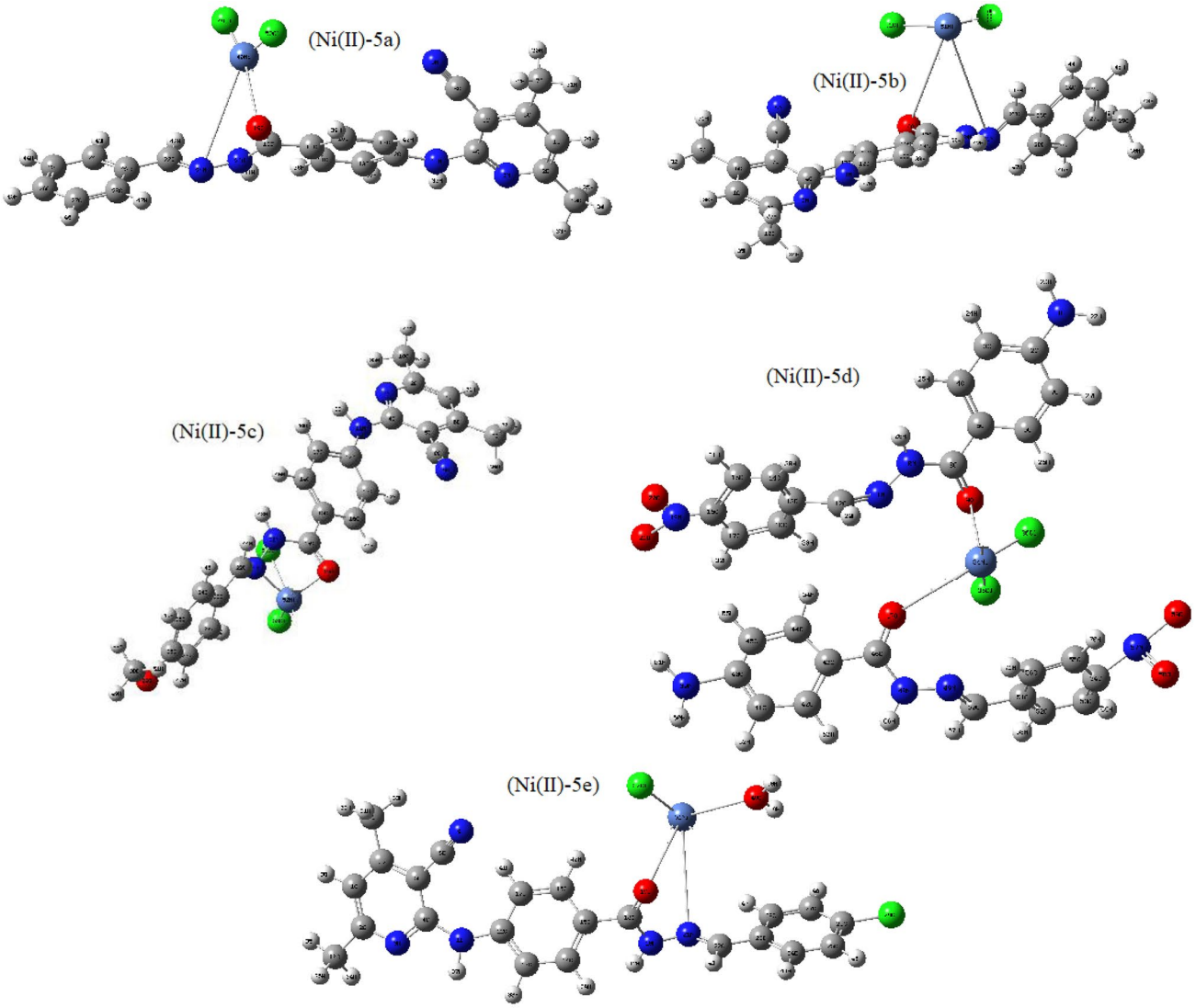

Fig. 1 The optimized structures of Ni(II) complexes

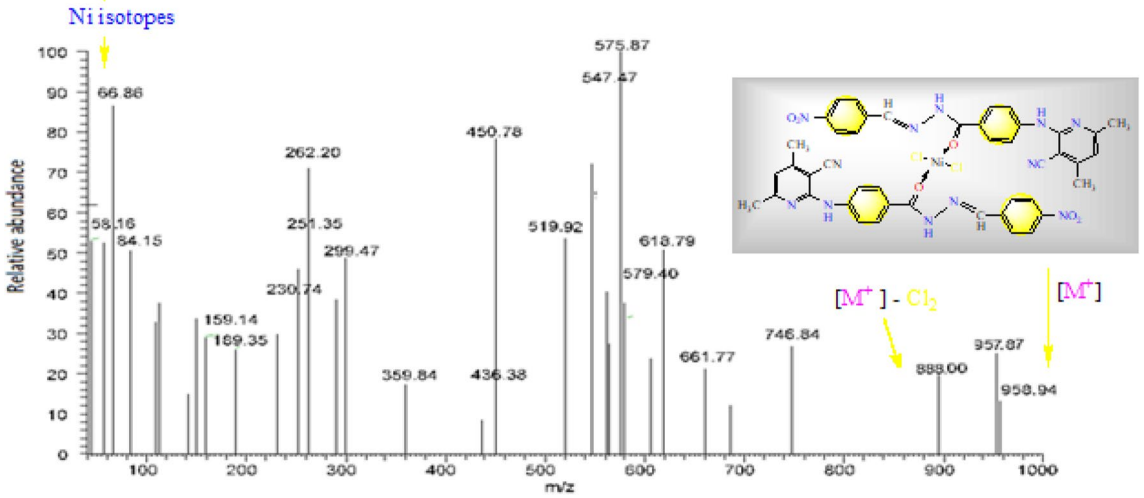

Fig. 2 Mass spectrum of Ni(II)-5d complex

3.4 Mass Spectral-Analysis

The further molecular conformation was conducted by mass spectral analysis under 40 °C min^{-1} heating rate at 70 eV over 50–1000 m/*z* range. Such-identification tool was carried out by using electron-spray for collision-induced ionization followed by fragmentation. For instance, Ni(II)-5d and Ni(II)-5e complexes, were the investigated examples (Figs. 2 and 3S), which accordingly confirm the rest. Whereas, the molecular ion peaks were appeared at *m/z* = 958.94 (I = 14%) and 534.34 (I = 12%) and match with M^+ and ($M^+ + 1$)-H_2O ions, respectively. The reduced intensity of molecular ion peaks is a normal feature for instability of molecular ion that leads to fragmentation [40]. The base peak recorded with the Ni(II)-5d and Ni(II)-5e complexes spectra, were *m/z* = 575.87 and 334.83, respectively that coincided with bulky molecular ions inside the coordination sphere. The most powerful peaks that corresponding to metal ion isotopes, which signify and confirm the complexation process. Such peaks undoubted appeared close to *m/z* ≈ 60 that verifying the presence of nickel atom.

3.5 TGA Analysis

This analytical tool interested in details for quality of binding inside the coordination sphere, particularly with solvent molecules. This analysis was conducted for all complexes at 10 °C min^{-1}, as a heating rate under nitrogenous atmosphere covering 20–800 °C range. All endothermic degradation stages, were appeared extended to cover four to five stages (Fig. 6S). The thermal stability of investigated complexes appeared varied but instability prevailed, except for Ni(II)-5d and Ni(II)-5e complexes. The water molecules proposed attached with most complexes, were strictly verified over the first degradation stage by matched mass-losses (found and calculated). Regarding thermal-degradation behavior over all investigated complexes was relatively-fixed in degradation behavior. So, the decomposition pathway was easily established over all stages and displayed (Table 4). The residual part recorded at ≈ 600 °C was NiO molecule, which sometimes polluted with carbon atoms.

3.6 XRD Analysis

Such analysis which dealing with the topography and crystal-lattice dynamic [41] evaluates the magnitude of crystallinity over three complexes (as example). Extracted patterns that displayed in Figs. 3 and 5S over $10° < 2\theta < 80°$ range, appeared having extent of nano-crystallinity. So, crystallite parameters were estimated by using known equations through FWHM method [42] (Table 5). FWHM, particulate size, 2θ, d spacing, relative intensity, crystal strain (ε) and dislocation density (δ), were the parameters calculated. The estimated sizes were appeared in 5.79–11.53 nm range, which signify their distinguish nanometer characteristics. The reduced crystal strain and dislocation density, enhanced the extent of regularity in crystal building and atomic packing. Miller indices (hkl) were obtained from VESTA software [43] based on known equations [44]. Such indices were 100, 103 and 130. This axial indices close to tetragonal feature with threefold symmetry that remains unchanged by rotation.

3.7 CT-DNA Binding Study

Applying spectrophotometric titration method, the binding quality of tested Ni(II) complexes against CT-DNA was tested (Fig. 8S). This investigation reflects a shadow

Table 4 Thermogravimetric analysis for Ni(II)-Schiff base complexes

Complexes	Steps	Temp. range (°C)	Decomposed	Weight loss; calcd. (found %)
(1) $[NiCl_2(HL)]\cdot 2H_2O$	1st	40.84–100.80	$-2H_2O+Cl_2-$	19.99 (19.95)
	2nd	110.81–368.56	$-C_6H_5$	14.41 (14.44)
	3rd	368.57–384.16	$-C_7H_7N$	19.65 (19.66)
	4th residue	410.18–524.40	$-C_9H_7N_4NiO$	31.99 (32.02)
				13.96 (13.93)
(2) $[NiCl_2(HL)]\cdot 2H_2O$	1st	26.34–96.89	$-2H_2O+0.5Cl_2$	13.02 (13.00)
	2nd	96.89–320.15	$-0.5Cl_2+CH_4$	9.38 (9.36)
	3rd	320.15–385.82	$-C_7H_7N$	19.13 (19.14)
	4th residue	385.82–530.31	$-C_{11}H_{10}N_4$	36.10 (36.08)
			$NiO+4C$	22.35 (22.42)
(3) $[NiCl_2(HL)]\ H_2O$	1st	35.34–105.02	$-H_2O$	3.29 (3.30)
	2nd	200.1–361.00	$-Cl_2$	12.96 (12.93)
	3rd	361.23–379.95	$-C_9H_8ON$	26.72 (26.70)
	4th residue	380.21–530.02	$-C_{13}H_{12}N_2$	35.87 (35.88)
	5th residue	530.06–559.60	$-CHN_2NiO$	7.50 (7.50)
				13.65 (13.69)
(4) $[NiCl_2(HL)_2]$	1st	270.11–380.34	$-Cl_2$	7.40 (7.42)
	2nd	396.58–410.94	$-C_{15}H_{12}N_3O_2$	27.78 (27.80)
	3rd	411.250–492.33	$-C_{12}H_{10}N_4O_3$	26.94 (26.95)
	4th residue	492.53–518.35	$-C_{13}H_{14}N_5$	25.07 (25.06)
			$NiO+4C$	12.81 (12.77)
(5) $[NiCl(HL)(H_2O)]Cl$	1st	151.37–316.56	$-H_2O+0.5Cl_2$	9.69 (9.70)
	2nd	317.74–328.47	$-Cl_2+C_7H_5$	29.02 (29.00)
	3rd	328.65–559.21	$-C_{14}H_{12}N_3$	40.30 (40.27)
	4th residue	559.30–572.24	$-CHN_2NiO$	7.44 (7.45)

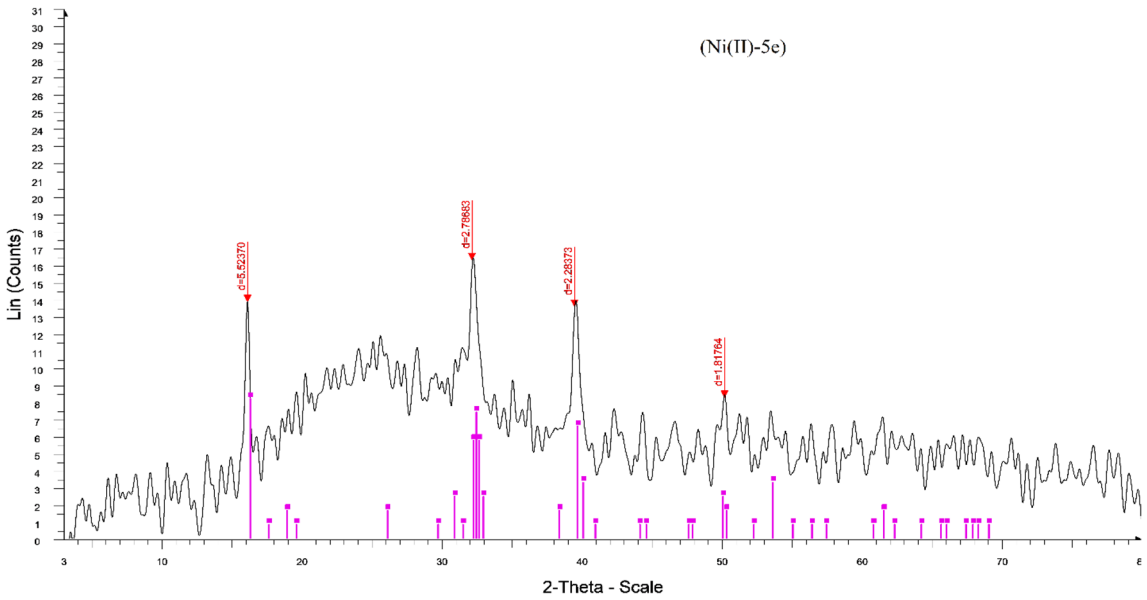

Fig. 3 XRD pattern of Ni(II)-5e complex

Table 5 Crystallographic data applying FWHM method for fairly crystalline complexes

Compounds	Size (Å)	2θ	Intensity	d-spacing (Å)	ε	δ ($Å^{-2}$)	FWHM	hkl
(1) Ni(II)-5c	1.15315	24.601	35.3	3.61576	0.37627	0.56624	1.28534	100
(2) Ni(II)-5d	0.57893	25.385	13.8	3.50585	0.72672	2.98365	2.56410	103
(3) Ni(II)-5e	0.80725	32.092	16.4	2.78683	0.41428	1.53456	1.86667	130

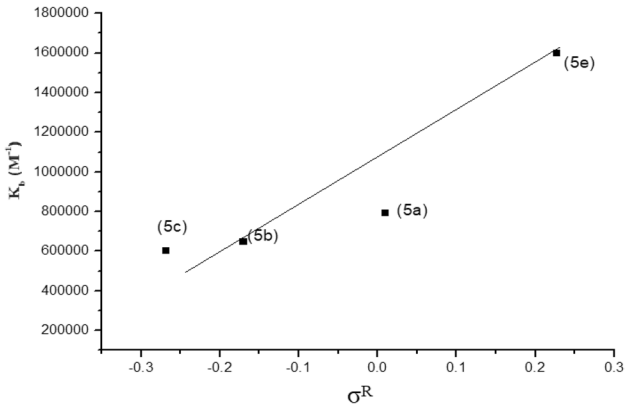

Fig. 4 The relation between Hammett coefficient (σ^R) and intrinsic binding constant (K_b)

on the degree of blocking for DNA-active sites by influence of tested complexes, which lead to its control inside infected cell. Intersect-binding constant (K_b) was extracted for four complexes based on an observable hyper-chromic shift in charge transfer band (≈ 350 nm) by 2–3 nm. This shift was observed clearly with increasing DNA amount over constant complex-concentration. The binding feature may be of electrostatic attraction or occlusion inside grooves appeared from helix-deterioration. The magnitude of hyper-chromic shift, as a result for extended complex structure, which primates electrostatic attraction with DNA-active sites. Also, the occlusion of binding-complex inside minor or major grooves that appeared through re-organizing DNA helix or fractional damage for double helix-surface. The binding constants (K_b, M^{-1}) for treated Ni(II) complexes were estimated utilizing known equations [45]. The values calculated were as follow; 2.6×10^5, 6.48×10^5, 6.02×10^5 and 1.6×10^6 For the complexes Ni(II)-5a, Ni(II)-5b, Ni(II)-5c and Ni(II)-5e complexes, respectively. This values matched perfectly with the magnitude of inductive effect of p-substituents, which attached such effect with binding efficiency. Hammett's equation [46], clarifies the direct relation between σR and binding efficiency (K_b) (Fig. 4). The high inductive effect of substituted groups that conducts to lack of electron-density over fictional-groups and led to intensive binding towards DNA-helix.

3.8 Computational Studies

3.8.1 Conformational Study

This computational study has a great impact on verifying the mode of bonding within the complexes. This based on the distribution of functional groups upon the optimum structures of the ligands. After geometry optimization process, the position of donor sites may facilitate or hinder their contribution in coordination. Such may considered the further asserting tool for the bonding inside the complexes, which really achieved (see Sect. 3.8.1.2). Accordingly, Gaussian09 software under DFT/B3LYP method was applied upon the ligands and their Ni(II) complexes. All synthesizes were faced configuration under economical basis set (3-21G) until executing optimization process that yielded the structural-forms

Table 6 Calculated physical parameters (eV) over optimized structures by RTD-B3LYP-FC method

Compound	E_H	E_L	E_H-E_L	E_l-E_h	*x*	μ	η	S (eV^{-1})	ω	σ
5a-BDAB	−0.20926	−0.06109	−0.1482	0.14817	0.135175	−0.13518	0.074085	0.037043	0.12332	13.49800904
Ni(II)-5a	−0.17248	−0.11584	−0.0566	0.05664	0.14416	−0.14416	0.02832	0.01416	0.366916	35.31073446
5b-CDAB	−0.20834	−0.05756	−0.1508	0.15078	0.13295	−0.13295	0.07539	0.037695	0.117228	13.26435867
Ni(II)-5b	−0.2114	−0.15277	−0.0586	0.05863	0.182085	−0.18209	0.029315	0.014658	0.565495	34.11222923
5c-CDMB	−0.20809	−0.05413	−0.154	0.15396	0.13111	−0.13111	0.07698	0.03849	0.111651	12.99038711
Ni(II)-5c	−0.15518	−0.09868	−0.0565	0.0565	0.12693	−0.12693	0.02825	0.014125	0.285154	35.39823009
5d-CDNB	−0.21147	−0.16498	−0.0465	0.04649	0.188225	−0.18823	0.023245	0.011623	0.76207	43.0200043
Ni(II)-5d	−0.16953	−0.15997	−0.0096	0.00956	0.16475	−0.16475	0.00478	0.00239	2.83918	209.2050209
5e-CCDB	−0.21039	−0.06742	−0.143	0.14297	0.138905	−0.13891	0.071485	0.035743	0.134956	13.98894873
Ni(II)-5e	−0.20965	−0.11101	−0.0986	0.09864	0.16033	−0.16033	0.04932	0.02466	0.260601	20.2757502

Table 7 Physical features from log-computational files

Compounds	E (A.U.)	D (Debye)	∫	E (nm)
5a-BDAB	– 1192.13013113	8.0854	0.0096	412.64
Ni(II)-5a	– 3608.73158143	7.3830	0.0001	10,007.7
5b-CDAB	– 1231.23496620	7.7742	0.0263	402.39
Ni(II)-5b	– 3649.37588157	16.2385	0.0014	3632.92
5c-CDMB	– 1306.02532742	8.1461	0.0021	396.38
Ni(II)-5c	– 3723.04756272	20.9262	0.0007	3750.88
5d-CDNB	– 1395.05339417	12.3260	0.0032	2226.33
Ni(II)-5d	– 4375.99044406	6.0932	0.0002	14,931.1
5e-CCDB	– 1649.51968224	9.1640	0.0228	423.88
Ni(II)-5e	– 3686.25740693	9.0534	0.0003	2481.73

displayed (Figs. 1 and 9S). In addition to, important files (log and chk) were excreted that feed us with essential characteristics for treated compounds (Tables 6, 7). Regarding chk files and implementing HOMO–LUMO energy band splitting (ΔE), functional physical-indexes were calculated (Table 6) and frontier-orbital images were also extracted (Figs. 5 and 10–11S). According to HOMO and LUMO images and with respect to Schiff base derivatives (Fig. 10S), intensive appearance for such molecular orbitals around hydrazide-moiety that responsible for coordination, was recorded. This signifies the extent of facility in electronic transitions among the coordinating groups. Moreover and according to HOMO and LUMO images of Ni(II) complexes (Figs. 5 and 11S), appeared fairly localized in metal atom and surrounding. This points to the influence of metal atom on electronic distribution over the whole compound, which lead to easiest electronic transition at all.

3.8.1.1 Functional Physical Parameters Electronegativity (x), chemical potential (μ), global-hardness (η), global-softness (s), global-electrophilicity (ω) and absolute-softness (σ), were the physical parameters calculated for all synthesizes

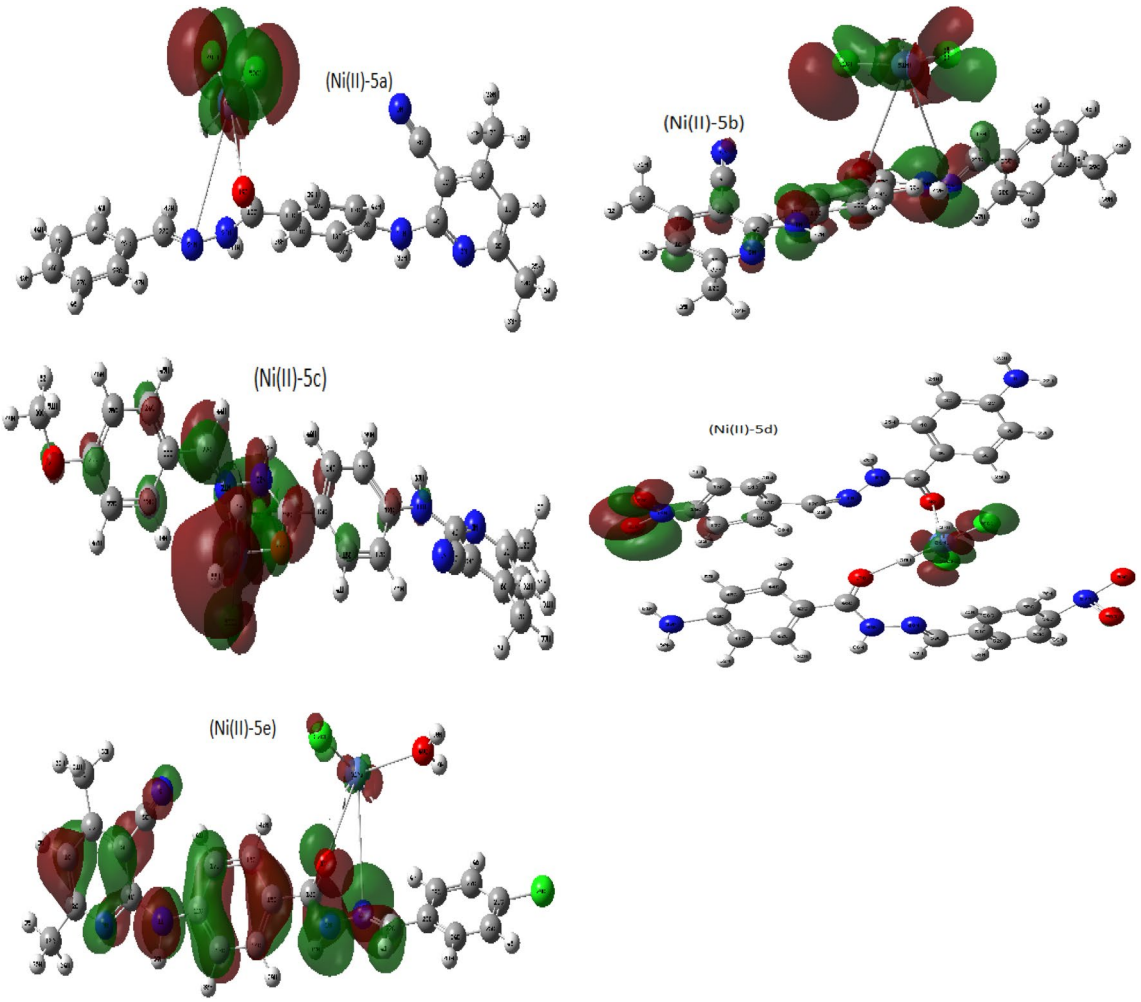

Fig. 5 HOMO images of Ni(II)-Schiff base (**5a–e**) complexes

to build their functional vision. Based on HOMO–LUMO energy band splitting (E_{LUMO}-E_{HOMO}) such parameters were estimated using known relations [22, 23]. From comparative point of view, regarding such parameters and with respect to Schiff base derivatives (**5a–e**), we notice the following; (i) the p-substituent impact was remarked clearly through the significant difference among the whole parameters. (ii) The favored characteristics (x, s, ω and σ) that orient to excellent properties, displayed the priority of (**5d**) derivative, which already has the powerful p-substituted group (nitro). While and with respect to Ni(II) complexes, we noticed the following; (i) general enhancement was recorded for all characteristics based on reduced ΔE values, in comparing with free ligands. (ii) Preferred electronegativity and softness properties were progressed with Ni(II)-5d upon the rest complexes. This demonstrates the positive influence of inductive-effect for p-substituent on functional-characteristics. Such priority points to promising biological feature, which coincides directly with the softness and electrostatic properties [47, 48]. (iii) Electrophilicity index (ω) was appeared varied significantly among Ni(II)-complexes, which also confirms the impact of substituents on that. Ni(II)-5d exhibited high electrophilicity, which already expected based on shortage in electron-density, which accompanied by high electron-acquiring ability from surrounding [49]. Dipole moment, excitation-energy, oscillator-strength and formation energy, were the other physical parameters extracted from log files after optimization process (Table 7). According to dipole moment values, were agreed successfully with p-substituent-behavior, which already varied covering donating (Me and OMe) and withdrawing (Cl and NO_2) groups. The reduced dipole moment value was recorded with Ni(II)-5d complex in compatible with electrophilicity feature. The values of excitation energy and oscillator strength, exhibited enhanced superiority of complexes in stability and bond-strength towards excitation process. Finally and according to formation energy values, appeared very compatible and weighted for advanced stability of complexes.

3.8.1.2 Molecular Electrostatic Potential (MEP) Electron-cloud maps (Figs. 6, 10S and 12S) were demonstrated over the atoms after building new cube over new surface-maps, to illustrate the magnitude of electron density over the molecule. The maps discriminate nucleophilic and electrophilic sites, by blue and red colors, respectively, while the middle-feature appeared green. The electrostatic maps of Schiff base derivatives (**5a–e**) (Fig. 10S), appeared by extensive range ($\approx \pm 9.8 \times 10^{-2}$) with favorable focus on amide and hydrazide centers. Such promotes their nucleophilic contribution towards Ni(II) ion [25]. While, the electrostatic maps of Ni(II) complexes, display extended range ($\approx \pm 0.16 \times 10^{2}$), exceeded free derivatives especially with Ni(II)-5b and Ni(II)-5c complexes. This exceeding may refer to the contribution of covalent-chloride as electron-dense atoms beside the role of p-substituents, which cannot ignored.

3.8.2 Quantitative Structural Characteristic Relationships Study

This computational study (QSAR) is a key player in judging on reactivity-magnitude of treated compound, towards the intended application. Such study was executed after energy minimization upon HyperChem (8.1) program, for all Ni(II) complexes. Under semi-empirical (AM1) setup that followed by Molecular Mechanics force field (MM^{+}) [14–17], the treatment was done without fixation for any parameter till equilibrium. The use of Polake-Ribiere conjugated gradient algorithm method [50], conducts to energy minimization characteristic. Surface area, hydration energy, reactivity, polarizability and log p were the QSAR parameters obtained (Table 8). Generally, promising feature can be expected easily for such complexes based on distinguish QSAR values, particularly the reactivity and Log p values. As known, a strong revers relation between partition-coefficient (log P) with that of biological activity [16, 17, 51]. So finally, Ni(II)-5d, Ni(II)-5e and Ni(II)-5c may offer vigorous results in biological application.

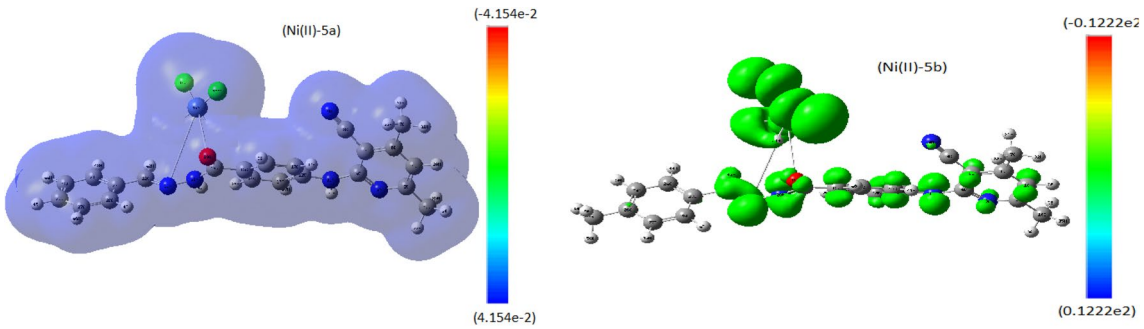

Fig. 6 Electrostatic maps for selected Ni(II)-Schiff base complexes (Color figure online)

Table 8 QSAR parameters for optimized Ni(II) complexes

The parameters	Ni(II) complexes				
	5a	**5b**	**5c**	**5d**	**5e**
Surface area (grid) (Å)	725.77	745.57	757.99	779.07	735.66
Volume (Å)	1228.00	1276.14	1302.43	1548.27	1256.84
Hydration energy (k cal mol^{-1})	− 11.50	− 10.64	− 13.61	− 37.82	− 22.42
Log p	1.86	2.02	0.87	-6.24	0.03
Reactivity (Å)	132.92	137.21	139.30	181.81	133.90
Polarizability (Å)	46.89	48.73	49.37	63.10	47.67

Table 9 Docking parameters for all synthesizes against breast cancer protein (3s7s)

Complex	Ligand	Receptor	Interaction	Distance (Å)	E (kcal mol^{-1})	S (energy score)
5a-BDAB	N9	ND2 ASN 136 (A)	H-acceptor	3.05	− 0.8	− 6.3019
Ni(II)-5a	O19	OE2 GLU 129 (A)	H-donor	2.95	− 3.02	− 6.5992
	N9	N GLY 117 (A)	H-acceptor	3.14	− 2.2	
	6-ring	N LYS 119 (A)	pi-H	3.84	− 1.6	
5b-CDAB	–	–	–	–	–	− 8.7869
Ni(II)-5b	O19	O MET 68 (A)	H-donor	2.69	− 17.2	− 6.527
	N21	O LYS 473 (A)	H-donor	3.52	− 0.9	
	N9	NZ LYS 230 (A)	H-acceptor	3.9	− 0.9	
	6-ring	N LYS 473 (A)	pi-H	4.03	− 1.1	
5c-CDMB	O19	N GLY 117 (A)	H-acceptor	3.31	− 0.7	− 6.3326
	O19	NZ LYS 376 (A)	H-acceptor	2.88	2.3	
Ni(II)-5c	O19	OE2 GLU 129 (A)	H-donor	2.86	− 3.6	− 6.9311
	N9	N GLY 117 (A)	H-acceptor	3.18	− 1.7	
	6-ring	N LYS 119 (A)	pi-H	3.79	− 1.7	
5d-CDNB	N11	OE2 GLU 129 (A)	H-donor	2.96	− 5.7	
	N20	O GLY 117 (A)	H-donor	3.02	− 2.1	− 7.1906
Ni(II)-5d	O32	NE2 GLN 296 (Q)	H-acceptor	3.10	− 2.7	− 9.1921
5e-CCDB	N20	SG CYS 437 (A)	H-donor	3.32	− 3.3	− 8.3743
	N9	CA VAL 373 (A)	H-acceptor	3.66	− 0.7	
	N9	N MET 374 (A)	H-acceptor	3.52	2.1	
Ni(II)-5e	O52	O GLU 274 (A)	H-donor	2.75	− 4.0	− 6.9734
	N9	NZ LYS 150 (A)	H-acceptor	3.20	− 1.1	
	6-ring	CA ASP 277 (A)	pi-H	4.23	− 0.9	

3.8.3 MOE-Docking Approach Study

This study is the exclusive technical approach in drug designing industry, which offer virtual view simulate the interaction between tested compound (proposed drug) and cell pathogen protein [15]. Molecular Operating Environmental module (vs. 2015) was used to accomplish such simulation for all investigated Ni(II) complexes against crystal structure of breast-cancer protein(3s7s). The ligand interaction parameters (Table 9), interaction validity patterns and surface-mapping (Figs. 7 and 13S) were extracted for each complex. Ligand types, receptors, interaction feature, H-bonding length, energy content in addition to scoring energy, were the interaction parameters used to evaluate the extent of inhibition. Comparative insight upon Schiff base-3s7s complexes (**5a–e**), offers the following remarks; (i) according to ligand binding sites, were focused on N9, 11, 20 and O19 atoms. (ii) According to receptor types, Asparagine, Glycine, Lysine, Glutamate, Cysteine, Valine and Methionine were the contributing amino acids in interaction patterns. (iii) According to interaction types, H-donor and H-acceptor were the only exhibited by true binding approach with length ≤ 3.5 Å [16, 17]. (iv) Finally and according to scoring energy values (kcal mol^{-1}), derivatives 5d (− 7.1906) and 5e (− 8.3743) displayed superior inhibition score. With respect to Ni(II)-Schiff bases-3s7s complexes, the following remarks were aggregated; (i) the interacting sites were, O32, 52; N9,19, 21 and 6-ring. (ii) Regarding

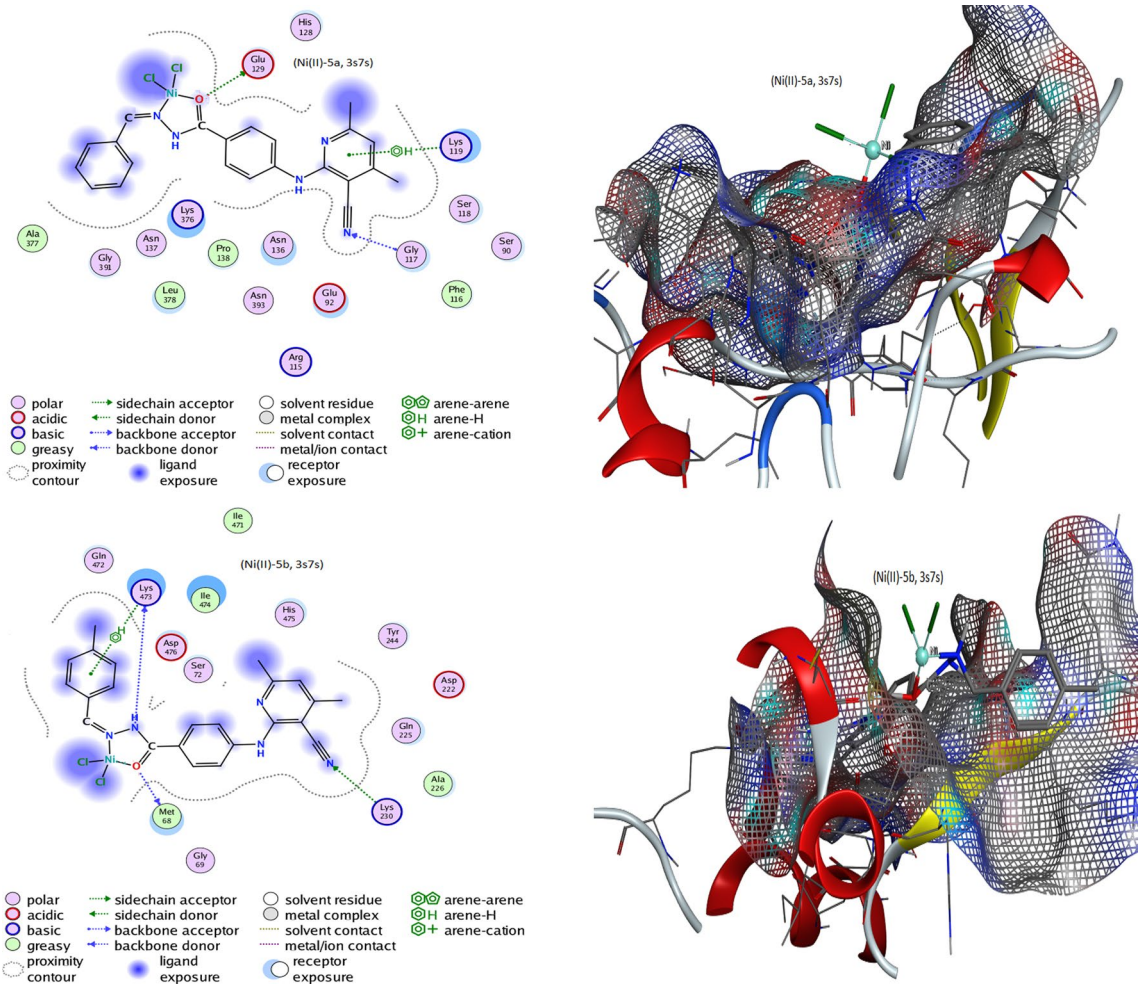

Fig. 7 Docking patterns and surface maps of Ni(II)-Schiff base (**5a–e**) complexes against 3s7s protein

receptor types contributing inside interaction patterns were, Glycine, Lysine, Glutamate, Glutamine, Aspartate and Methionine. (iii) Regarding the interaction types actually considered, were H-donor, H-acceptor and pi-H that having real lengths. (iv) Finally and regarding scoring energy values, Ni(II)-5d, Ni(II)-5c and Ni(II)-5e complex exhibited superior inhibition score against breast cancer protein (3s7s) [25]. With respect to interaction validity patterns as well as surface-mapping (Figs. 7 and 13S), we noticed that, the receptor exposure has prevalence over ligand-exposure. Also, the interaction types were covered all polar, acidic, basic and greasy beside a broad proximity-contour surrounding the tested compound.

3.9 In-Vitro Anticancer Screening

As we know that, the scientific research faces a great challenge towards overcoming cancer daises particularly, breast cancer which annually leads to death of many women. Consequently, we concerned with in-vitro screening for new synthesized Ni(II) complexes, against breast cancer cell line (MCF-7). The inhibition efficiency was tested for series of concentrations from each tested complex as; 12.5, 25, 50 and 100 µM, to estimate the IC_{50}. Doxorubicin, which is known by its distinct anti-tumor efficiency, was the reference drug used for comparison. This comparison facilitates ranking the inhibition-attitude among the whole tested compounds and then throw a light on that promising. Demonstrating a relationship between the concentration (µg ml^{-1}) and cell-viability (%), leads to estimatingIC_{50} (µg ml^{-1}) values as mentioned in Table 10. The values displayed superiority of Ni(II)-5e and Ni(II)-5c complexes, which appeared having very strong inhibition towards breast-cancer cell line. Also, Ni(II)-5d has a significant inhibition but the rest displayed moderate activity.

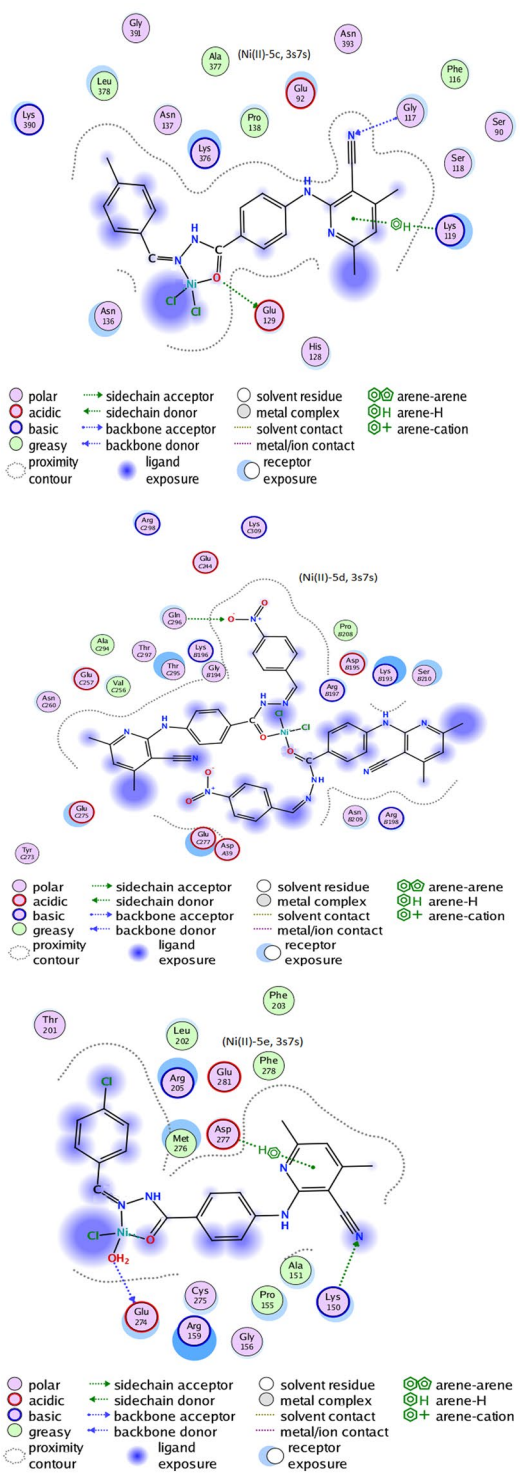

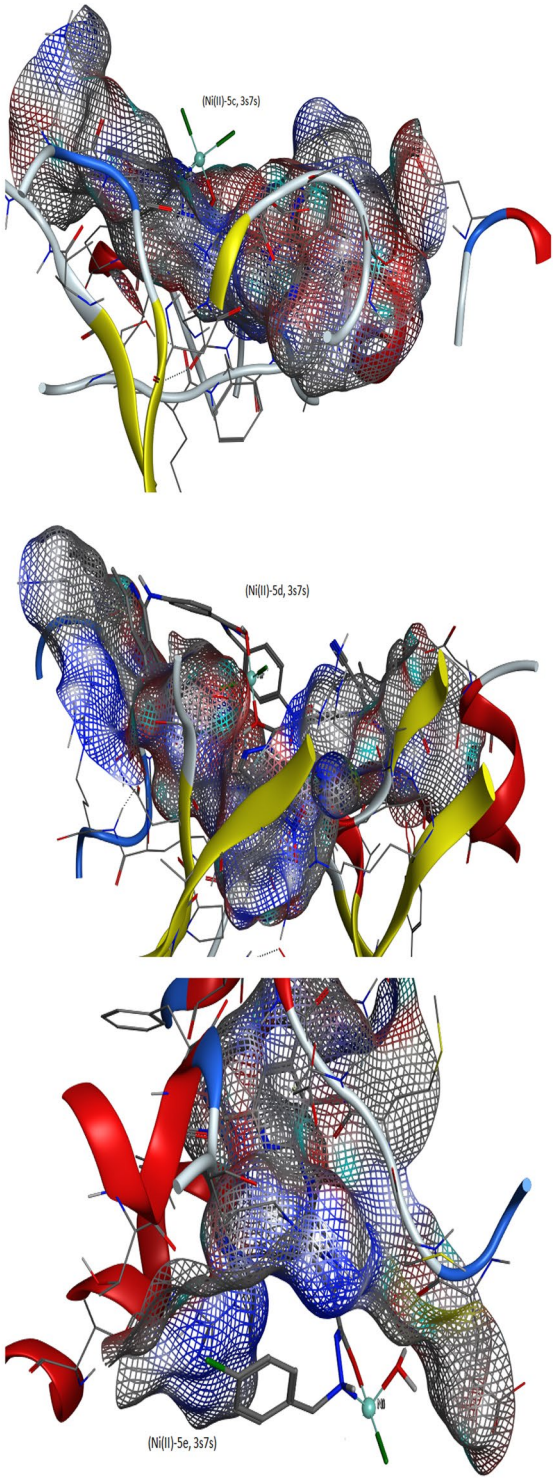

Fig. 7 (continued)

Table 10 Antitoxic activity of Ni(II) complexes against MCF-7 cell line

Complexes	In vitro cytotoxicity IC_{50} (μg ml^{-1})
Doxorubicin	26.1 ± 0.2
(1) $[NiCl_2(HL)] \cdot 2H_2O$	46.92 ± 2.9
(2) $[NiCl_2(HL)] \cdot 2H_2O$	41.03 ± 2.1
(3) $[NiCl_2(HL)] \cdot H_2O$	27.61 ± 1.6
(4) $[NiCl_2(HL)_2]$	32.63 ± 1.5
(5) $[NiCl(HL)(H_2O)]Cl$	22.73 ± 1.4

4 Conclusions

Novel Ni(II)-Schiff base complexes were prepared and characterized. The mode of bonding was strongly affected by p-substituents features. The structural formula appeared steady with all Ni(II) complexes by square-planer form. The conformational study was implemented to establish the best atomic distribution inside the structures. The docking simulation was applied for all complexes against breast-cancer protein. After simulation process, expected distinguish characteristic was recorded with most treated complexes. In-vitro screening was tested for all Ni(II) complexes, against MCF-7 cell line. Promising inhibition activity was recorded with Ni(II)-5c and Ni(II)-5e complexes.

Compliance with Ethical Standards

Conflicts of interest The authors declare no conflict of interest.

References

1. F. Xu, W. Li, W. Shuai, L. Yang, Y. Bi, C. Ma, H. Yao, S. Xu, Z. Zhu, J. Xu, Eur J. Med. Chem. **173**, 1–14 (2019)
2. C.S. McCrae, A. Ross, A. Stripling, N.D. Dautovich, Clin. Interv. Aging **2**, 313–326 (2007)
3. T.S. Harrison, L.J. Scott, Drugs **65**, 2309–2336 (2005)
4. X. Wang, G. Mick, K. McCormick, Physiol. Rep. **7**, e14151 (2019)
5. A.M. Al-Majid, M.S. Islam, S. Atef, F.F. El-Senduny, F.A. Badria, Y.A.M.M. Elshaier, M. Ali, A. Barakat, A.F.M. Motiur Rahman, Molecules **24**, 1332 (2019)
6. Y.-L. Zhang, F.-Q. Zhao, J. Inorg. Organomet. Polym. **28**, 2714–2720 (2018)
7. H.C. Wang, X.Q. Yan, T.L. Yan, H.X. Li, Z.C. Wang, Molecules **21**, 1012 (2016)
8. F.A. Saad, M.G. Elghalban, N. El-Metwaly, H. El-Ghamry, A.M. Khedr, Appl. Organometal. Chem **31**, e3721 (2017)
9. D.C. Culita, L. Dyakova, G. Marinescu, T. Zhivkova, R. Spasov, L. Patron, R. Alexandrova, O. Oprea, J. Inorg. Organomet. Polym. **29**, 580–591 (2019)
10. H.A. El-Boraey, M.A. El-Salamony, J. Inorg. Organomet. Polym. **29**, 684–700 (2019)
11. X.-L. Wan, L. Dong, J.-Z. Wang, H.-T. Shi, L.-B. Yang, J. Inorg. Organomet. Polym. **29**, 1184–1191 (2019)
12. R.W.-Y. Sun, D.-L. Ma, E.L.-M. Wong, C.-M. Che, Dalton Trans. **43**, 4884–4892 (2007)
13. K.L. Haas, K.J. Franz, Chem. Rev. **109**, 4921–4960 (2009)
14. H.A. Katouah, J.H. Al-Fahemi, M.G. Elghalban, F.A. Saad, I.A. Althagafi, N.M. El-Metwaly, A.M. Khedr, Mater. Sci. Eng. C **96**, 740–756 (2019)
15. F.A. Saad, N.M. El-Metwaly, A.M. Khedr, J. Inorg. Organomet. Polym. **29**, 1606–1624 (2019)
16. N. El-Metwaly, I. Althagafi, H.A. Katouah, J.H. Al-Fahemi, T.M. Bawazeer, A.M. Khedr, Appl. Organomet. Chem. **33**, e5095 (2019)
17. I. Althagafi, M.G. Elghalban, N.M. El-Metwaly, J. Inorg. Organomet. Polym. (2019). https://doi.org/10.1007/s10904-018-01062-3
18. J. Marmur, J. Mol. Biol. **3**, 208–2018 (1961)
19. A. Wolfe, G.H. Shimer, T. Meehan, Biochemistry **26**, 6392–6396 (1987)
20. M.J. Frisch et al., *Gaussian 09, Revision D* (Gaussian Inc., Wallingford, CT, 2010)
21. R. Dennington II, T. Keith, J. Millam, *GaussView, Version 4.1.2* (Semichem Inc., Shawnee Mission, KS, 2007)
22. R.C. Chikate, S.B. Padhye, Polyhedron **24**, 1689 (2005)
23. R.F. George, Eur. J. Med. Chem. **47**, 377 (2012)
24. M.H. Abdellattif, M.A. Hussien, E. Alzahrani, Int. J. Pharm. Sci. Res. **9**, 1000–1019 (2018)
25. I. Althagafi, N. El-Metwaly, T.A. Farghaly, Molecules **24**, 1741 (2019)
26. T. Mosmann, J. Immunol. Methods **65**, 55–63 (1983)
27. F. Denizot, R. Lang, J. Immunol. Methods **89**, 271–277 (1986)
28. R.R. Weichselbaum, H.J. Mauceri, N.N. Hanna, M.A. Beckett, D.H. Gorski, M.-J. Staba, K.A. Stellato, K. Bigelow, R. Heimann, S. Gately, M. Dhanabal, G.A. Soff, V.P. Sukhatme, D.W. Kufe, Nature **394**, 287–291 (1998)
29. A.I. Vogel, *Text Book of Quantitative Inorganic Analysis* (Longman, London, 1986)
30. W.J. Geary, J. Coord. Chem. Rev. **7**, 81–122 (1971)
31. A. Yassin, Chem. Heterocycl. Compd. **45**, 35–41 (2009)
32. M.S. Morales-Ríos, P.Y. López-Camacho, O.R. Suárez-Castillo, P. Joseph-Nathan, Tetrahedron Lett. **48**, 2245–2249 (2007)
33. J. Song, H. Yamataka, Z. Rappoport, J. Fluor. Chem. **124**, 119–122 (2003)
34. K.S. Abu-Melha, N.M. El-Metwally, Spectrochim. Acta A **70**, 277–283 (2008)
35. N.M. El-Metwaly, R.M. El-shazly, I.M. Gabr, A.A. El-Asmy, Spectrochim. Acta A **61**, 1113–1119 (2005)
36. A.B.P. Lever, *Inorganic Electronic Spectroscopy* (Elsevier, Amsterdam, 1986)
37. N.M. El-Metwally, G.A.A. Al-Hazmi, Spectrochim. Acta A **107**, 289–295 (2013)
38. N.M. El-Metwally, K.S. Abu-Melha, Transit. Met. Chem. **32**, 828–834 (2007)
39. A.A. Abou-Hussen, N.M. El-Metwaly, E.M. Saad, A.A. El-Asmy, J. Coord. Chem. **58**, 1735–1749 (2005)
40. M.S. Refat, N.M. El-Metwaly, Spectrochim. Acta A **81**, 215–256 (2011)
41. B.D. Cullity, *Elements of X-Ray Diffraction*, 2nd edn. (Addison-Wesley, Reading, 1993)
42. S. Velumani, X. Mathew, P.J. Sebastian, S.K. Narayandass, D. Mangalaraj, Sol. Cells **76**, 347–358 (2003)
43. K. Momma, F. Izumi, J. Appl. Crystallogr. **44**, 1272–1276 (2011)
44. B.D. Cullity, S.R. Stock, *Elements of X-Ray Diffraction*, 3rd edn. (Prentice Hall, New Jersey, 2001)

45. A.Z. El-Sonbati, A.F. Shoair, A.A. El-Bindary, M.A. Diab, A.S. Mohamed, J. Mol. Liq. **209**, 635–647 (2015)
46. L.H. Abdel-Rahman, A.M. Abu-Dief, N.M. Ismail, M. Ismael, J. Inorg. Nano-Met. Chem. **47**, 467–480 (2017)
47. G.A. Al-Hazmi, K.S. Abou-Melha, N.M. El-Metwaly, K.A. Saleh, Bioinorg. Chem. Appl. **2018**, 7176040 (2018)
48. H. Allal, Y. Belhocine, E. Zouaoui, J. Mol. Liq. **265**, 668–678 (2018)
49. I. Fleming, *Frontier Orbital's and Organic Chemical Reactions* (Wiley, London, 1976)
50. M.M. Al-Iede, J. Karpelowsky, D.A. Fitzgerald, Pediatr. Pulmonol. **51**, 394–401 (2016)
51. N. El-Metwaly, J.H. Al-Fahemi, I. Althagafi, A.M. Khedr, H.A. Katouah, J. Inorg. Organomet. Polym. (2019). https://doi.org/10.1007/s10904-019-01233-w

Publisher's Note Springer Nature remains neutral with regard to jurisdictional claims in published maps and institutional affiliations.